The Meteoritical Society

Meteoritics & Planetary Science 43, Nr 7, 1219–1231 (2008)
Abstract available online at http://meteoritics.org

Aragonite in the Murray (CM2) carbonaceous chondrite: Implications for parent body compaction and aqueous alteration

Martin R. LEE[1*] and Rachael ELLEN[2]

[1]Department of Geographical and Earth Sciences, University of Glasgow, Gregory Building, Lilybank Gardens, Glasgow G12 8QQ, UK
[2]School of Earth and Environment, University of Leeds, Leeds LS2 9JT, UK
[*]Corresponding author. E-mail: martin.lee@ges.gla.ac.uk

(Received 09 August 2007; revision accepted 05 February 2008)

Abstract–The matrix of the CM2 carbonaceous chondrite Murray contains rare micrometer-sized prismatic crystals of aragonite that formed during late-stage parent body aqueous alteration. The aragonite was identified by X-ray microanalysis coupled with electron backscatter diffraction (EBSD), TEM selected area electron diffraction and cathodoluminescence spectroscopy. The sixteen crystals found all occur within loose and elongate submillimeter-sized clusters and one cluster is present in each of the two thin sections studied. Orientation determinations using EBSD show that the *c* axes of aragonite crystals within each cluster lie roughly in a plane, itself aligned approximately parallel to the long axis of the host cluster. Aragonite is inferred to have crystallized after calcite but before completion of static/impact-related compaction. The clusters developed by growth of aragonite within films of aqueous fluids that had a relatively high Mg/Ca ratio. These fluids were focused within zones of high porosity and permeability along a weak compactional fabric in the matrix and this fabric is also likely to have influenced the orientations of aragonite crystals as they grew. These results suggest that aragonite probably occurs in most of those carbonaceous chondrites that have undergone moderate degrees of parent body aqueous alteration and may provide further insights into the evolution of pore fluid compositions and volumes and the chronology of asteroidal evolution.

INTRODUCTION

The CM2 carbonaceous chondrites are a mineralogically and texturally complex and varied group of meteorites that characteristically contain a suite of minerals including phyllosilicates, hydrous sulfides, carbonates, and sulfates that formed during parent body aqueous alteration (see Brearley 2006a for a recent review). The task of unraveling the history of aqueous alteration is challenging and some aspects remain poorly understood, for example the temperature and chemistry of the pore fluids and the mechanisms by which they interacted with the parent body. Although carbonate minerals are a volumetrically minor constituent of the CM2s (Fuchs et al. 1973; Bunch and Chang 1980), their chemical and isotopic compositions are an important source of information on the absolute chronology of aqueous alteration (e.g., Brearley and Hutcheon 2002) and the provenance and evolution of the host fluids (Grady et al. 1988; Johnston and Prinz 1993; Riciputi et al. 1994; Benedix et al. 2003). The majority of this work has focused on calcite, which is the dominant carbonate in CM2s (Johnson and Prinz 1993; Brearley et al. 1999, 2001), but both aragonite and dolomite have also been reported (Müller et al. 1979; Barber 1981; Johnson and Prinz 1993; De Leuw et al. 2007). The information that the latter two minerals can provide on the alteration history of their parent rocks has yet to be fully realized owing to the limited number of petrographic, chemical and microstructural studies of these minerals that have been undertaken to date.

During a survey of the microstructures of Ca-carbonates in a number of CM2 meteorites using electron backscatter diffraction (EBSD) (Conolly et al. 2007), clusters of micrometer-sized aragonite crystals were discovered in the matrix of Murray. This is the first report of aragonite in a CM2 meteorite since the transmission electron microscopy (TEM) work of Barber (1981) and the presence of this mineral is of particular note owing to its metastability with respect to the much more abundant calcite (Zolensky 2001). Here we describe the petrographic context, microstructure and composition of Murray aragonite and use this information to explore the temperature and chemistry of ambient solutions and the structure of the meteorite matrix during crystal growth. The results show that despite, and possibly by virtue of, its very low volumetric abundance, this mineral can

provide important new insights into the late-stage evolution of the parent body and in particular temporal changes in volumes and compositions of pore fluids and in the nature of their interaction with the fine-grained meteorite matrix.

MATERIALS AND METHODS

This study used two polished thin sections of Murray that were obtained from the Natural History Museum (London): BM1966,48, P13114 and P13115, both with a surface area of ~27 mm^2. Prior to electron microscopy each thin section was re-polished for a total of ~1 minute using colloidal silica then coated with a thin layer of carbon. BSE imaging, qualitative energy-dispersive X-ray microanalysis (EDX), EBSD mapping and cathodoluminescence (CL) imaging all used a FEI Quanta 200F field-emission SEM operated at 20 kV. The SEM is equipped with an integrated EDAX-TSL EDX-EBSD system and a KE Developments Centaurus panchromatic CL detector. Note that all BSE and CL images and EBSD maps of each thin section were acquired with the sample in the same orientation (i.e., the thin section was moved only in X and Y between images or scans) in order to facilitate comparisons of the crystallographic orientations of aragonite crystals with each other and with various structures in the meteorite.

EBSD work was undertaken with the thin section and stage tilted at 70° towards the EBSD camera. The indexing of the Kikuchi patterns was optimized by means of the Hough transform, typically using fifteen bands with a 3° tolerance, and the structure files were constructed from the standard unit-cell parameters of aragonite (space group *Pmcn*: a = 0.496 nm, b = 0.797 nm, c = 0.574 nm) and calcite (space group $R\,\bar{3}c$: a = 0.499 nm, c = 1.7062 nm). All of those Ca-carbonate grains analyzed by EBSD produced good Kikuchi patterns and so were crystalline. For acquisition of EBSD maps from individual crystals the scanning parameters were tailored to their size and typical scan areas were ~100 μm^2, acquisition rates were ~5–10 patterns/s with step sizes of ~0.2 μm, which yielded ~3000–7000 indexed patterns over acquisition times of ~20–30 minutes. As each area scanned typically included some of the meteorite matrix the data sets were cleaned by removal of those points with a low confidence index. Orientation data are here plotted in the lower hemisphere of equal angle pole figures. Each point in these figures represents the orientation of the pole to a particular plane relative to three reference directions, two orthogonal directions in the plane of the thin section (TD and RD) and one normal to its surface (ND). Thus a crystal oriented such that (001) lies parallel to the surface of the thin section will plot in the centre of a {001} pole figure (i.e., at ND). Larger areas of the thin sections were also mapped by EBSD in an attempt to locate aragonite crystals and these maps were acquired from areas of ~0.35 mm^2 at a step size of ~0.9 μm, giving ~500,000 indexed patterns over collection times of ~19 hours. The mapping of even larger areas at a resolution sufficient to identify micrometer-sized aragonites would have required prohibitive instrument time.

CL images were obtained from both aragonite and calcite using the Quanta SEM and they reveal spatial variations in emission intensities over the entire 300–650 nm wavelength range of the bialkali photomultiplier, although it is most sensitive to the shorter (UV and blue) wavelengths (Lee et al. 2005). CL emission spectra and quantitative chemical analyses of the Ca-carbonates were acquired using a Cameca SX100 electron probe at the University of Strathclyde that is equipped with three wavelength-dispersive X-ray spectrometers (WDX) and a silicon CCD spectrograph that analyses light collected via the microprobe's optical microscope. The CCD has 1024 columns and a 400 line/mm diffraction grating and produces spectra from 336–852 nm with a point spacing of ~0.5 nm. Background corrected emission spectra were acquired over 2 seconds and at room temperature with the microprobe operated at 15 kV/10 nA and using a 2 μm spot. Further details of the spectroscopy are provided by Lee et al. (2005) and Edwards et al. (2007). For quantitative chemical analyses the electron probe was operated at 15 kV/10 nA and with a 5 μm spot. Standardization used calcite (for calcium), periclase (for magnesium), rhodonite (for manganese) and pyrite (for iron); preliminary analytical work showed that strontium was below the limits of detection. Counting times on peak and background were 30 and 15 sec. respectively and detection limits were approximately 0.05 wt% $MgCO_3$ and 0.18 wt% $MnCO_3$ and $FeCO_3$. As noted by Johnson and Prinz (1993), EPMA work on carbonate minerals in carbonaceous chondrites is challenging owing to their small size (limiting the degree to which the beam can be defocused) coupled with the low concentrations of trace elements that are typically present. To have obtained better detection limits would have necessitated greater counting times, which coupled with the small spot size would have exacerbated the considerable beam damage during each analysis. Most of the aragonites were too small to yield reliable chemical analyses using the 5 μm spot and given our desire to preserve as many of the sixteen crystals as possible for future work, only the largest of the aragonites (M29) was analyzed by EPMA.

The microstructure of one of the aragonites in P13115 (crystal M21) was additionally investigated by cutting an electron-transparent foil from the crystal using a FEI XT Nova Nanolab dual-beam focused ion beam (FIB) instrument. The milling used a 30 kV Ga^+ ion beam throughout and the method employed here for cutting foils from meteorites in thin section has been described by Lee et al. (2003) and Lee and Smith (2006). After milling, the foil was extracted from the thin section using an in situ micromanipulator and welded to the edge of a copper grid using ion beam-deposited platinum. Although FIB milling can damage minerals by Ga^+ ion implantation and heating (Lee et al. 2007) it is very unlikely that such artifacts could

transform calcite to aragonite and previous work has confirmed that calcite retains its crystallinity and crystal structure throughout FIB milling (Heaney et al. 2001). The initial low-voltage scanning transmission electron microscope imaging of the foil used the Quanta 200F SEM (Lee and Smith 2006), then diffraction-contrast images and selected area electron diffraction (SAED) patterns were acquired using a FEI T20 TEM operated at 200 kV.

RESULTS

Composition and Mineralogy of Murray

Murray fell in Kentucky in 1950 and in common with many other CM2 meteorites is a regolith breccia (McSween 1979a; Rubin and Wasson 1986) that has undergone parent body aqueous alteration. McSween (1979b) found that it was "partially altered," Hanowski and Brearley (2000) refer to it as one of the "least altered" CM2 meteorites and Rubin et al. (2007) classified it as a CM2.4/2.5. Murray contains a variety of clasts including a CO-like clast and millimeter-sized CM2 clasts that have been variably aqueously altered (Bunch and Chang 1980; Rubin and Wasson 1986) and magnetite-rich CI-like clasts were also found in the present study. The two thin sections contain CAIs, chondrules and chondrule fragments, most of which have fine-grained rims, also called "accretionary dust mantles" by Metzler et al. (1992) and "dark-mantles" by Trigo-Rodríguez et al. (2006), between which is a fine-grained matrix containing a variety of mineral grains and aggregates. SEM point counting showed that P13115 contains 59.8 vol% matrix (including fine-grained rims), 13.2 vol% serpentine-tochilinite, 13 vol% anhydrous silicate, metal and sulfide grains and aggregates, 11.9 vol% intact chondrules and 2.3 vol% Ca-carbonate. Ca-carbonate only was point counted in P13114 and comprised 1.6 vol%. These data compare with a matrix abundance in Murray of 58.8 vol% determined by McSween (1979b) and volumes of serpentine-tochilinite of 29 ± 3 and ~5% found by Metzler et al. (1992) and Hanowski and Brearley (2000) respectively. Below we describe the two Ca-carbonate minerals found in the matrix of Murray, aragonite and calcite.

Aragonite Distribution, Microstructure, and Composition

The two thin sections have a combined area of ~54 mm^2 and contain sixteen micrometer-sized crystals of aragonite, giving an overall abundance of 0.004 vol%. These crystals were identified by EDX in combination with EBSD, with the software being able to select between aragonite and calcite for the best match with each Kikuchi pattern. The accuracy of this method of mineral identification was checked by manual indexing of SAED patterns obtained from the FIB-produced foil of M21. These SAED patterns index as aragonite and the orientations they provide are in excellent agreement with those obtained by EBSD mapping of the same crystal. CL emission spectra were also very different between those Ca-carbonates identified as aragonite and calcite using EBSD. Parts of zoned calcite crystals have a peak in the blue (~430 nm) whereas other areas have a broader orange peak (~600 nm), which are the "intrinsic" and Mn^{2+} activated emission bands respectively (Lee et al. 2005). By contrast, the aragonite crystals produce a single (green) peak at ~490 nm (Fig. 1). Green CL is characteristic of aragonite (Marshall 1988), although it is unclear from this previous work whether ~490 nm is the "intrinsic" luminescence of the mineral or is due to Mn^{2+} activation. Most of the aragonites were located by systematically combing the thin sections by high magnification BSE imaging and analyzing all potential aragonite crystals by EDX then EBSD. In order to confirm that very small aragonites or those with unusual habits had not been overlooked, high-resolution EBSD maps were acquired from several ~0.35 mm^2 areas but did not reveal any additional crystals. As part of a parallel study of the microstructures of Murray calcite, 42 grains were mapped by EBSD, but none contained aragonite inclusions.

All but one of the Murray aragonites are single crystals and most are euhedral. Those oriented with their *c* axes approximately normal to the plane of the section are equant and ~10–15 μm in size (Fig. 2a) whereas crystals whose *c* axes lie approximately in the plane of the thin section are prismatic, elongate parallel to *c*, and up to 75 μm in length (Figs. 2b, 3a and 3b). The dominant crystal faces are parallel to the traces of {110} with the minor faces parallel to the traces of {010} (Fig. 4a). This {110} prismatic habit is common to aragonite from a variety of terrestrial environments, for example speleothems (Frisia et al. 2002). One of the aragonites (M18) has split to form a crystallite that is not elongate along *c* but its faces are nonetheless parallel to traces of {110} and {010} (Fig. 2b). EBSD mapping showed that two of the crystals in P13115 (M21 and M28) contained a single twin that is ~0.7 μm wide on {001} and whose composition plane is parallel to the trace of {110} (Figs 2a, 4a, and 4b). The twinning can be described by a rotation of ~60° around <001> (Fig. 2a). These microstructures are considerably coarser than the ~100 nm scale twins described from CM2 aragonite by Barber (1981). TEM imaging also shows that the aragonite crystals have a relatively high density of point defects and a narrow fringe with an even greater density of defects where the crystal is in contact with fine-grained matrix (Figs. 4b and 4c). The aragonites were unzoned in panchromatic CL images and M29, the largest crystal found, has a mean composition determined by EPMA of 0.37 mole% $MgCO_3$ and 1.61 mole% $FeCO_3$ (n = 4 analyses) with manganese and strontium below detection limits.

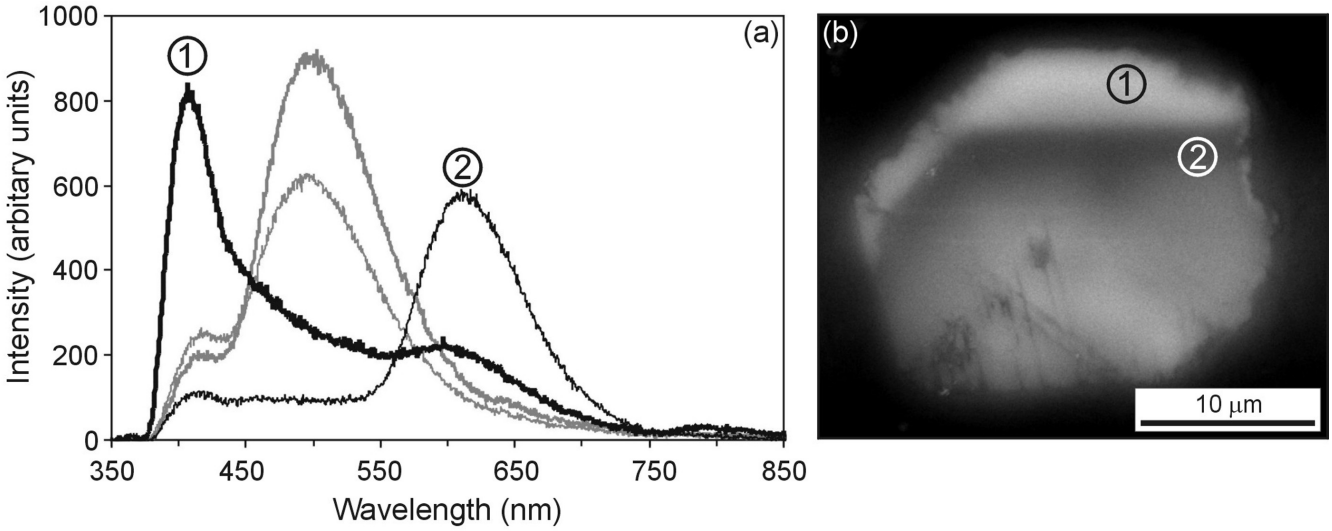

Fig. 1. CL results from Ca-carbonates in P13114. a) Emission spectra from a zoned calcite grain (black lines) and aragonite crystal M29 (grey lines). Calcite spectrum 1 has a peak in the blue and spectrum 2 has an orange peak whereas both aragonite spectra have one main peak in the green. b) Panchromatic CL image of the zoned calcite grain from which the two spectra in (a) were obtained. Those areas with the strongest panchromatic CL signal (i.e., white) have the greatest intensity of blue CL.

All of the aragonite crystals occur within the matrix and are surrounded by finely crystalline phyllosilicates or clumps of serpentine-tochilinite (Figs. 2 and 3). There is no evidence for replacement of aragonite by tochilinite, but in some cases matrix phyllosilicates fill embayments in the edges of the crystals (Figs. 3b and 4b). Note that the defect-rich fringe of M21 is continuous even around these embayments. Parts of some aragonite crystals are absent, leaving open pores (Fig. 3a), but it is difficult to determine whether the aragonite had dissolved within the parent body or had been plucked out during thin section preparation. Those crystals whose *c* axes lie approximately in the plane of the thin section are commonly cross-cut by fractures, along some of which there has been a few micrometers of displacement and these microfaults may also cut the surrounding fine-grained matrix and clumps of serpentine-tochilinite (Figs. 2a and 3b). The {001} pole figures show that there is very little difference in the orientation of pieces of the faulted grains, indicating that displacement has been accompanied by only minor rotation of the *c* axes of the pieces relative to each other (Fig. 3b).

In each of the two thin sections the aragonite crystals occur together in a loose cluster. The cluster in P13115 contains eleven crystals in an area of ~0.7 mm^2, nine of which occur within a 0.34 mm^2 region (Fig. 5). This cluster may itself be subdivided into upper and lower parts astride a clast, chondrule and a large chondrule fragment (Fig. 5). Aragonite crystals within the cluster have a weak preferred orientation, which is expressed by similarities in orientations of their *c* axes, but this is not seen in the {110} pole figures. The crystals are oriented with their *c* axes ranging from parallel to normal to the surface of the thin section and all but one plot in one of two quarters of the corresponding {001} pole figure (Fig. 5); the outlying point is from M57, which has been fractured (see below). The aragonite *c* axes therefore lie in a plane that is oriented approximately NE-SW relative to the thin section, which is similar to the alignment of the long axis of the host cluster and this correspondence is more apparent if the upper and lower clusters are considered separately. Importantly, the area of P13115 that contains the cluster also has some good evidence for compactional deformation and development of a fabric. A N-S oriented axis of compression can be inferred from plastic deformation of fine-grained rims between the chondrule and chondrule fragment separating the two parts of the cluster (Fig. 6a). Aragonite crystal M57 has also broken into two pieces in a style suggestive of fracturing in response to N-S oriented compression (Fig. 6b) and as a consequence the *c* axes of the two pieces differ significantly in orientation (Fig. 5). The area of P13115 that contains the lower cluster also has a well developed NE-SW fabric that is defined by the elongation of clumps of serpentine-tochilinite (Fig. 5). The cluster in P13114 comprises five crystals in an area of ~0.31 mm^2 (note that M31a and M31b are counted as individuals because their *c* axis orientations differ significantly, but they are sufficiently close that they may be pieces of a single broken crystal) (Fig. 7). The *c* axes of aragonites in this cluster are oriented at a low angle to the surface of the thin section and together lie in a plane that is aligned approximately E-W relative to the host meteorite (Fig. 7). In common with P13115, the plane containing the *c* axes of aragonite crystals is oriented roughly parallel to the long axis of the host cluster (Fig. 7).

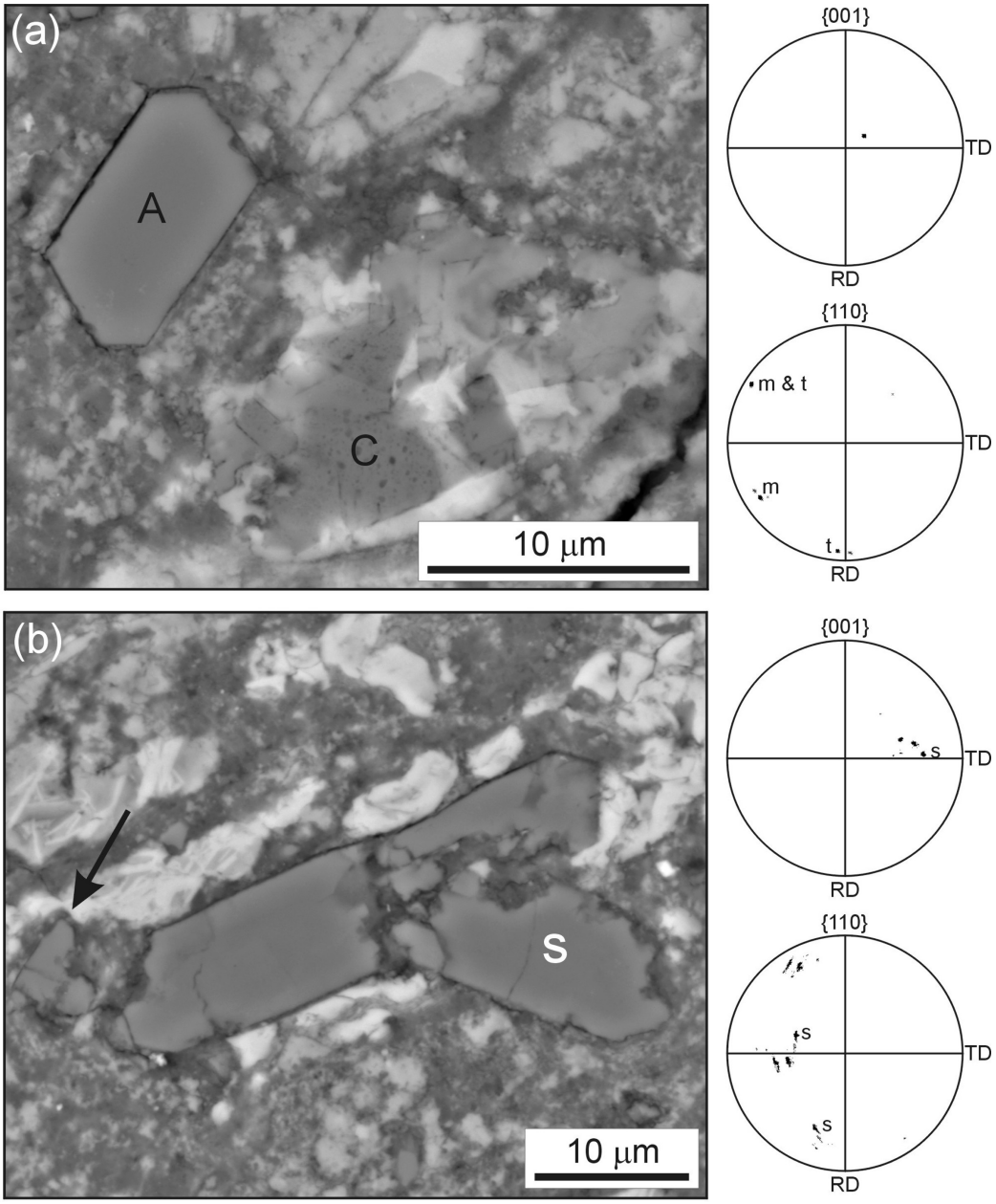

Fig. 2. BSE images of two aragonite crystals from P13115. The corresponding {001} and {110} lower hemisphere equal angle pole figures were obtained from EBSD maps of each crystal after removal of low confidence index points. a) Aragonite crystal M28 (A) whose *c* axis lies nearly normal to the plane of the thin section. The main faces of the crystal are parallel to the traces of {110} ("m" in the pole figure) and {010} and it is bisected by a narrow twin ("t" in the pole figure) whose composition plane is parallel to the trace of {110}. A small calcite grain (C) with a tochilinite rim (white) lies ~5 μm from the aragonite. Each pole figure contains 1070 data points. b) M18, the only split crystal found, the left hand end of which has been displaced by a microfault (arrowed). The main part of the crystal is elongate parallel to *c* and its faces are parallel to the traces of {110} whereas the long axis of the split (S) lies at an angle to *c* but its two main faces are again parallel to the traces of {110} ("s" in the pole figures). The clusters of data points in the {110} pole figure are smeared out as the scan has incorporated broken and displaced pieces of aragonite located at the end of the crystal and where the split meets the main part. The crystal is surrounded by fine-grained matrix (medium grey) and clumps of serpentine-tochilinite (white), which are clearly cross-cut by the aragonite. Each pole figure contains 3275 data points.

Petrography and Composition of the Calcite

Benedix et al. (2003) inferred both calcite and dolomite to be present in Murray from the volume of CO_2 liberated during acidification of crushed samples with H_3PO_4 at 25 °C and 100 °C, respectively. Only Ca-carbonates were found in the present study and EBSD and CL spectroscopy confirms that all grains inferred to be calcite from grain shape and petrographic

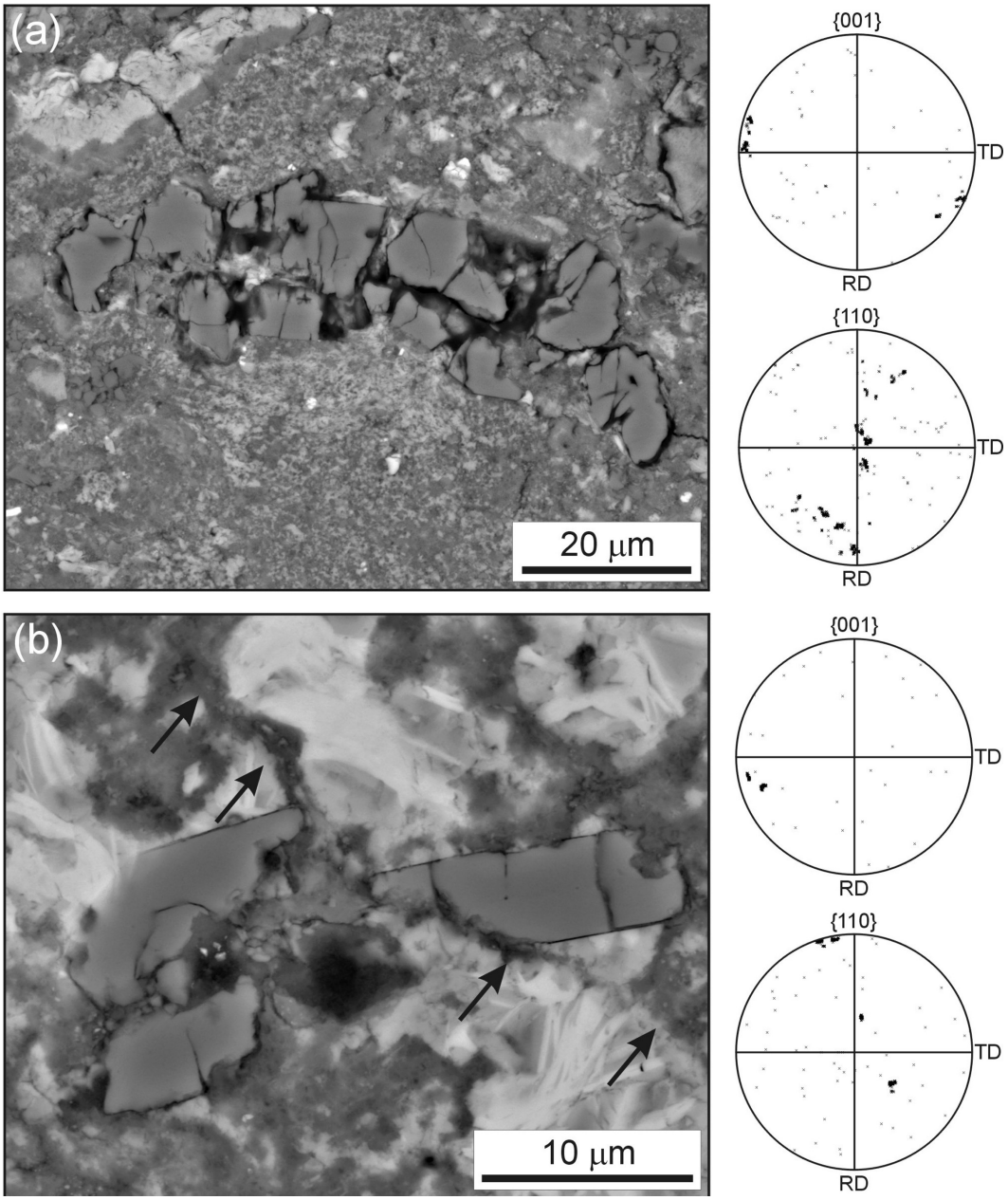

Fig. 3. BSE images of two aragonite crystals from P13114. The corresponding {001} and {110} lower hemisphere equal angle pole figures were obtained from EBSD maps of each crystal after removal of low confidence index points. a) M29, the largest aragonite crystal found in the two thin sections, which has been heavily fractured and pieces of the crystal have also been removed by parent body dissolution or thin section preparation. The fracturing and consequent minor displacement of pieces of the crystal is responsible for the smearing out of groups of points in the pole figures, especially {110}. Each pole figure contains 2300 data points. b) M30, which has been broken by microfaults, one of which can be traced from the serpentine-tochilinite through the aragonite (arrows) and has an apparent displacement of ~4 μm. The matrix fills small embayments in the crystal, for example at the right hand end. Each pole figure contains 800 data points.

context (described below) are indeed calcite. The two thin sections contain 1.6 and 2.3 vol% of calcite that is concentrated in the matrix, although it has previously been found in chondrules (Bunch and Chang 1980) and one CAI (Lee and Greenwood 1994). The calcite grains are 10–60 μm in size, anhedral (rounded) to subhedral in shape and are distributed fairly uniformly throughout the matrices of both thin sections. However, calcite is absent from the fine-grained rims and from a 1.0 by 0.6 mm sized area of the matrix of P13115, although this area was not obviously different to the matrix elsewhere in the thin section. Most calcite grains are associated with tochilinite, with or without intergrown serpentine, and the two minerals have a number of interrelationships, which in order of abundance are (i) one or more calcite crystals enclosed by a

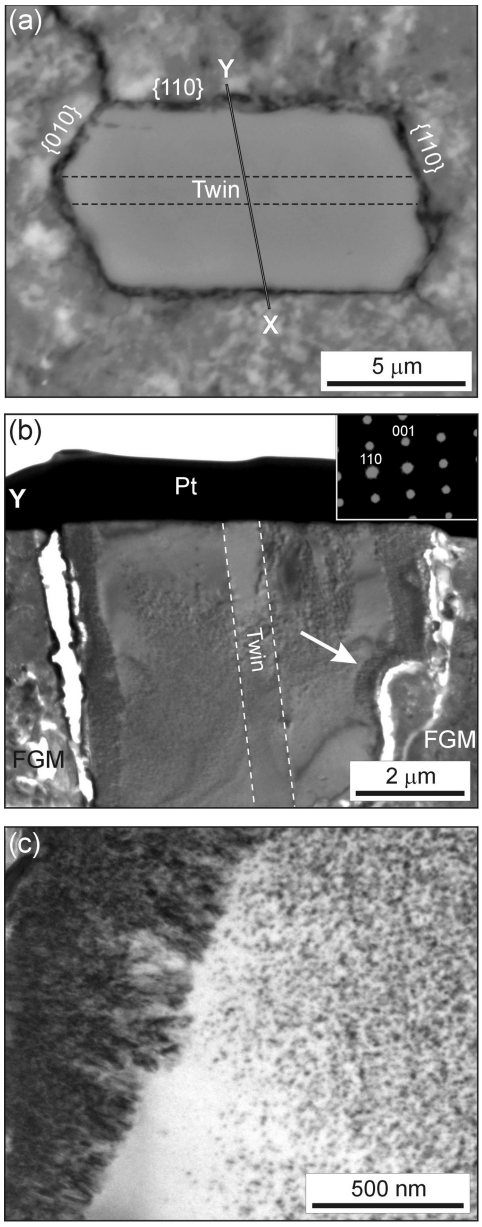

Fig. 4. Images of aragonite crystal M21 from P13115. a) BSE image of the crystal, which is bisected by a twin (edges marked by a pair of dashed lines). The orientations of crystal faces as determined by EBSD are indicated and line X-Y marks the midplane of a foil cut from this crystal using the FIB. b) Bright-field TEM image of the foil with an inset [$\bar{1}$10] SAED pattern, which confirms that the twin composition plane is parallel to the trace of {110} and the crystal surface lies close to {001}, in excellent agreement with orientations determined by EBSD. Y indicates the orientation of the foil relative to (a) and the edges of the twin are highlighted. The spotty contrast of the aragonite is due to abundant point defects and both edges of the crystal where in contact with the fine-grained matrix (FGM) have a very high defect density. Note that this defect-rich band is present even where the crystal is embayed by the matrix (arrow). Pt denotes the FIB-deposited layer of protective platinum. c) Bright-field TEM image of one side of the aragonite crystal illustrating the difference in defect density between the marginal defect-rich band (upper left hand side) and the interior of the crystal.

serpentine-tochilinite clump, (ii) tochilinite filling narrow fractures cutting the calcite, (iii) a thin and discontinuous rind of tochilinite surrounding the entire grain, (iv) one or more radial-fibrous tochilinite aggregates interpenetrating with calcite, and (v) individual acicular tochilinite crystals enclosed entirely by calcite. Some of these associations demonstrate clearly that the tochilinite postdates calcite. The majority of calcite grains have uniform contrast in panchromatic CL images or patchy variations in CL intensity. Only 4 out of 26 of grains imaged, all in P13114, displayed zoning consistent with crystal growth into a pore (Fig. 1b). CL spectroscopy shows that the grains have the "intrinsic" emission at ~430 nm and/or a broad Mn^{2+} peak at ~600 nm (Fig. 1a). The Murray calcite has a mean composition determined by EPMA of 0.18 mole% $MgCO_3$, 0.24 mole% $MnCO_3$ and 1.44 mole% $FeCO_3$ (n = 21 analyses from 7 grains).

DISCUSSION

Aqueous Alteration of CM2 Meteorites and Calcite Crystallization

Ca-carbonate minerals in the matrices of CM2 meteorites are widely believed to be products of parent body aqueous alteration (e.g., Kerridge and Bunch 1979) and results of the present study are consistent with the same origin for aragonite and calcite in Murray. There are a range of estimates of the compositions and temperatures of fluids that mediated alteration of CM2s, which have been reviewed by Brearley (2006a). Most studies have concluded that temperatures were relatively low (≤25 °C) (DuFresne and Anders 1962; Zolensky et al. 1993; Clayton and Mayeda 1999; Rosenberg et al. 2001), the solutions had a circumneutral to slightly alkaline pH (DuFresne and Anders 1962; Zolensky et al. 1993) and there was an initial water/rock ratio of 0.4–0.8 (Clayton and Mayeda 1999). In a recent study using clumped-isotope thermometry, Guo and Eiler (2007) found that carbonates in most analyzed samples of Cold Bokkeveld, Murchison and Murray crystallized from alkaline fluids at 20–35 °C, which is consistent with the previous work. Prior to discussing the potential origins of Murray aragonite it is necessary to discuss the timing of calcite growth and origin of the solutions from which it crystallized.

Calcite is inferred to have crystallized relatively early in the alteration history of CM2s (Brearley et al. 1999; Benedix et al. 2003) and Mn-Cr isotopic dating of calcite from Yamato (Y-) 791198 (CM2) suggests that it formed no more than 10 million years after the CAIs (Brearley et al. 2001). This chronology is consistent with calcite predating tochilinite in Murray and other CMs (Bunch and Chang 1980; Brearley 2006a) because tochilinite is a breakdown product of Fe,Ni metal and troilite, which would have been among the first minerals to have reacted with water (Rubin et al. 2007). However, as Brearley (1998) and Brearley et al. (2001) found

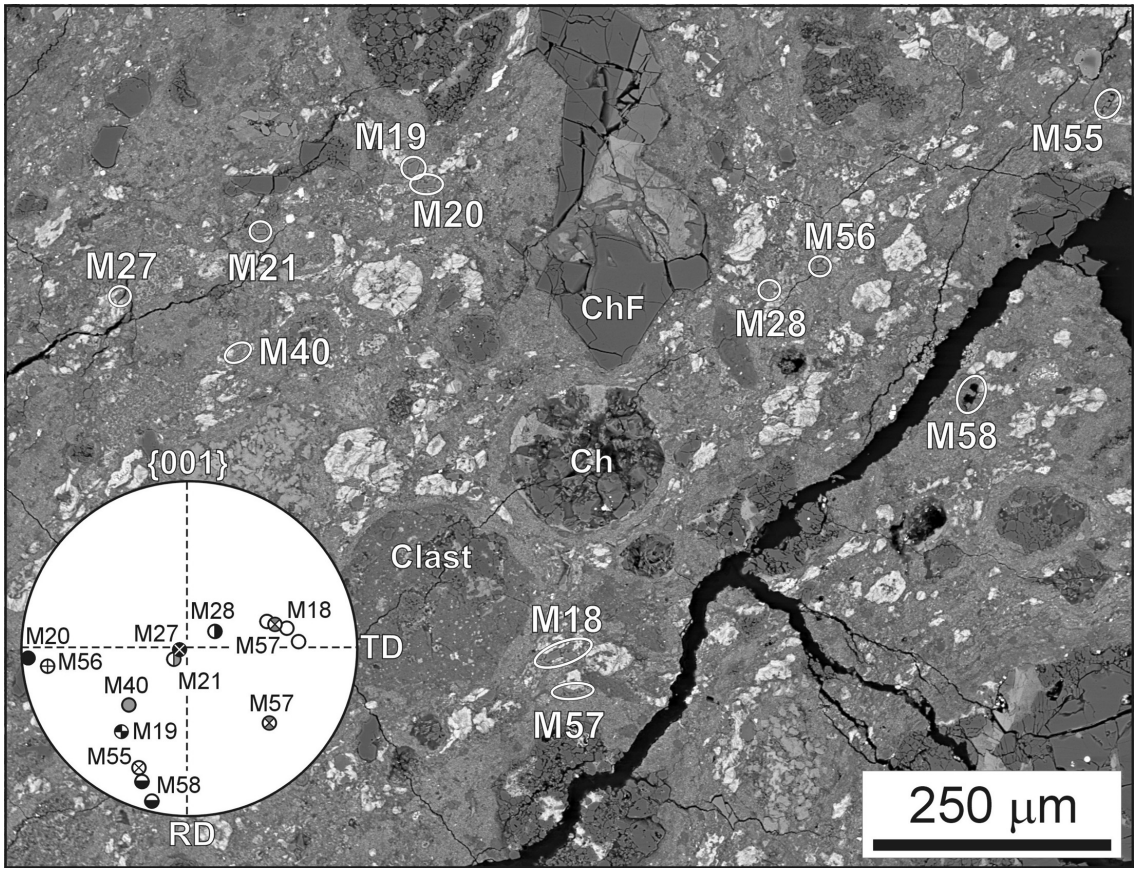

Fig. 5. BSE image of the aragonite cluster in P13115. Each of the 11 constituent crystals are ringed and labeled and their orientations as determined by EBSD are shown by the inset {001} pole figure. At least some of the range of orientations is attributable to rotation of grain pieces during breakage (e.g., M57). The cluster may be divided into upper and lower parts astride the clast, chondrule (Ch) and large chondrule fragment (ChF). Note that a NE-SW fabric can be recognized on either side of the NE-SW oriented fracture by elongation of serpentine-tochilinite clumps.

evidence for multiple phases of crystallization and dissolution of calcite in some CM2 meteorites, a proportion of the Murray calcite could have formed over an extended time period. Brearley (2006b) suggested that calcium for CM2 calcite was leached from chondrule mesostasis by low pH fluids. As the calcite grains are distributed fairly uniformly throughout the Murray thin sections (although the extent to which original grain distributions have been modified by brecciation and regolith gardening is unknown), once liberated from chondrules the calcium ions must have been transported through a water-saturated matrix on the mm-scale, either by diffusion through static solutions or by advection of the fluids themselves. The CL zoning of Murray calcite found in this study (Fig. 1b) and described from other CM2s (e.g., Brearley 1998; Brearley et al. 2001; Brearley 2002) indicates that at least some crystals grew into open pores and that concentrations of Mn^{2+} (together with other trace elements) in solution changed over time (Brearley 2006b). As zoning patterns can differ significantly between grains within a single thin section (Brearley 2002), the exchange of trace elements within Murray by diffusion or advection must have been slow relative to calcite crystallization rates. Thus, the majority of the calcite within Murray is inferred to have crystallized relatively early and from aqueous fluids that were widely distributed but poorly interconnected and whose concentrations of trace elements and saturation states varied significantly over time.

Relative Timing of Aragonite Crystallization

Determining the timing of aragonite crystallization relative to calcite is difficult owing to its scarcity and the absence of intergrowths of the two minerals. There is no evidence for replacement of aragonite by calcite, despite its metastability with respect to calcite at low pressures (Carlson 1980) and the widespread distribution of calcite-precipitating fluids, and so the aragonite is inferred to have formed later. As CM2 meteorites are noted for their disequilibrium mineral assemblages any conclusion based on relative mineral stabilities is necessarily tentative but this inferred timing is

consistent with Barber (1981), who found that aragonite postdated calcite in Cold Bokkeveld (CM2). As most aragonite crystals are euhedral and have sharp contacts with the surrounding matrix, they are also interpreted to have crystallized after serpentine-tochilinite and matrix phyllosilicates. Although the matrix cuts some crystal faces, the continuity of the defect-rich fringe around the phyllosilicate-filled embayment in M21 (Fig. 4b) argues against replacement and in favor of the aragonite having grown around an area of preexisting matrix. The fracturing and microfaulting of many aragonites shows that they crystallized prior to completion of static compaction of the parent body, or at least one phase of impact-related stress, but the very small displacement of the microfaults indicates that the magnitude of this stress was minor. This inference of a relatively late-stage timing of aragonite crystallization is consistent with models for the evolution of pore fluid chemistry within the CM2s as discussed below.

Compositions of Solutions in Equilibrium with Aragonite and Calcite

Despite the metastability of aragonite at low pressures, its occurrence in a wide variety of terrestrial environments such as shallow marine waters and caves, shows that the mineral can precipitate from aqueous fluids under Earth surface conditions, although it is readily replaced by calcite during burial diagenesis. Magnesium in solution plays an important role in the crystallization of aragonite from $CaCO_3$-supersaturated solutions because its adsorption on to calcite surfaces poisons active growth sites (Fernández-Díaz et al. 1996). Morse et al. (1997) undertook experiments using seawater based solutions to quantify the roles of magnesium concentrations and temperatures on the polymorph of $CaCO_3$ that precipitates inorganically. Using solution Mg/Ca values of up to ~5.5 and temperatures of up to ~35 °C they found that precipitation of calcite is favoured at all temperatures where Mg/Ca is <~0.5 and in low temperature (<~7 °C) waters at all values of Mg/Ca. Aragonite will precipitate as temperatures increase, at a constant Mg/Ca (where >~0.5), and as Mg/Ca increases at a constant temperature (where >~7 °C). Using results of ion microprobe analyses of Ca-carbonates from a range of CM2 meteorites, Riciputi et al. (1994) estimated that the solutions in equilibrium with calcite during its growth (or recrystallization) had temperatures of <20 °C and molar Mg/Ca values of ≤0.2 and terrestrial seawater with such properties would indeed crystallize calcite (Morse et al. 1997). Assuming the same partition coefficient for magnesium into calcite as used by Riciputi et al. (1994) (i.e., 0.044), solutions in equilibrium with Murray calcite would have had a molar Mg/Ca value of 0.04, which is in good agreement with the estimates from other CMs.

Using the experimental results of Morse et al. (1997) as a guide, the change from precipitation of calcite to aragonite within the Murray parent body could have been due to an increase in solution Mg/Ca from ~0.04 at a constant or increasing temperature. An increase in Mg/Ca would be expected in a chemically closed system if calcium were being removed from solution, for example by precipitation of low-Mg calcite, at a greater rate than magnesium. Morse et al. (1997) found that an increase in Mg/Ca during calcite precipitation often lead to calcite rhombs being overgrown by aragonite fibres and Barber (1981) found polycrystalline and dendritic aragonite overgrowing calcite in Cold Bokkeveld (CM2), which would be consistent with such a closed-system increase in Mg/Ca. Although aragonite and calcite are not in contact in Murray, the calculated molar Mg/Ca ratio of

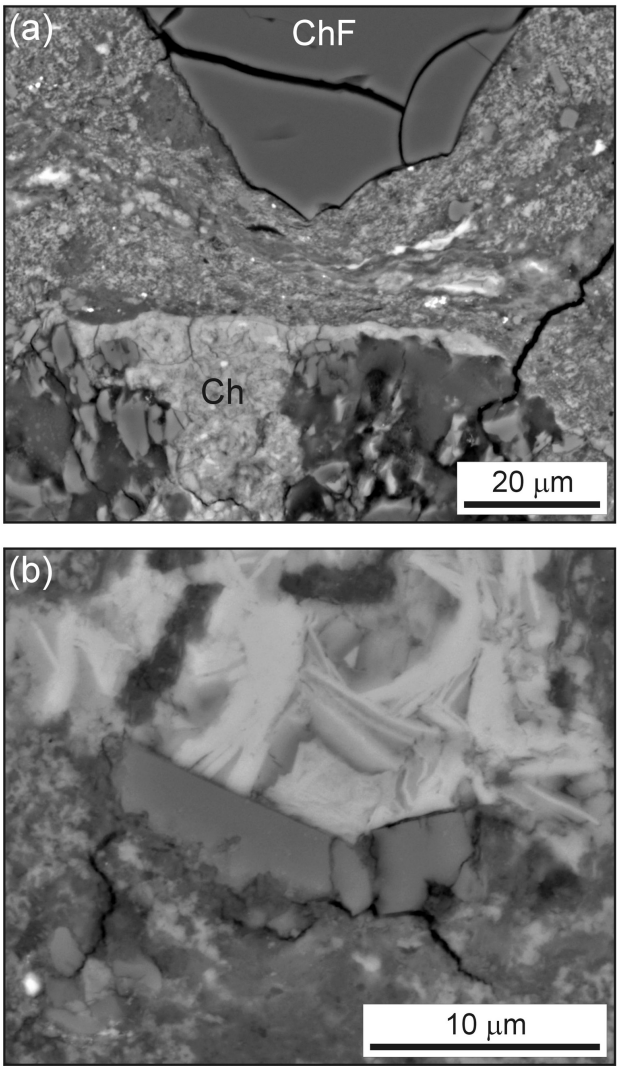

Fig. 6. BSE images of areas within the P13115 cluster. a) Plastic deformation of fine-grained rims between a chondrule (Ch) and chondrule fragment (ChF), which is suggestive of N-S oriented compression (from an area in the middle of Fig. 5). b) Aragonite crystal M57, which is surrounded by serpentine-tochilinite (above) and fine-grained matrix (below). The crystal has broken into two pieces in response to N-S oriented compression.

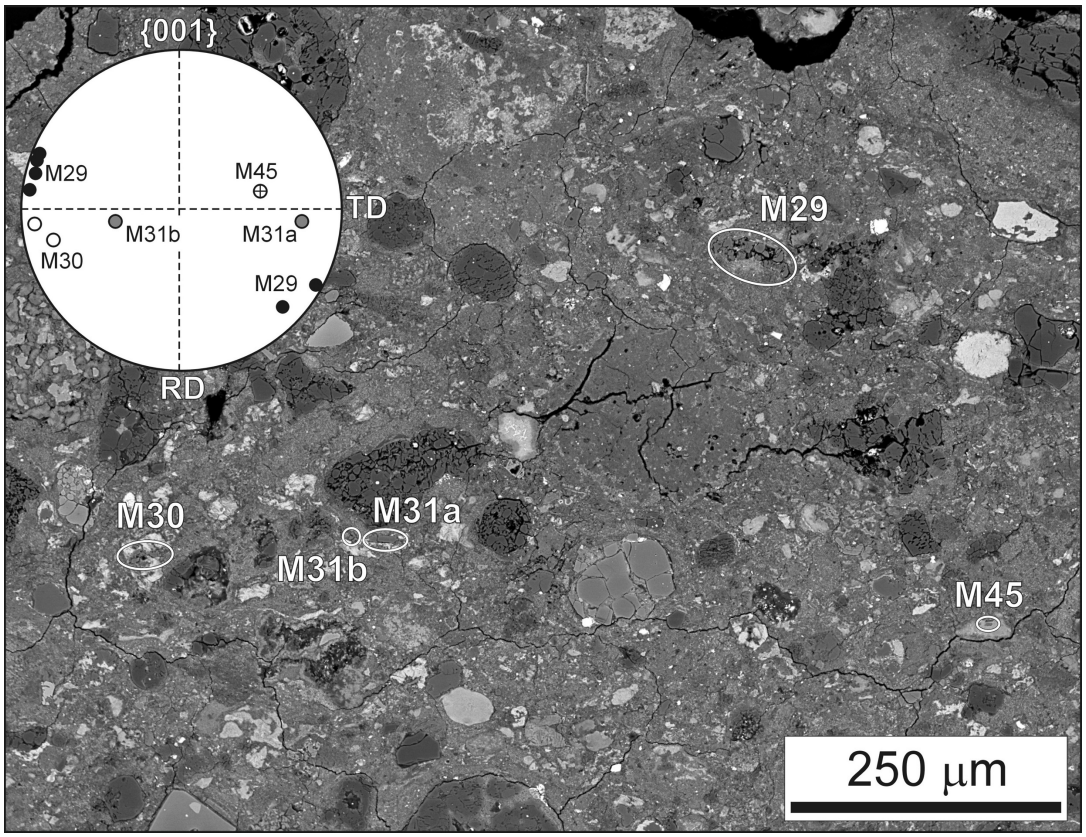

Fig. 7. BSE image of the aragonite cluster in P13114. Each of the five constituent crystals are ringed and labeled and their orientations as determined by EBSD are shown by the inset {001} pole figure.

solutions in equilibrium with aragonite crystal M29 is 2.92, assuming a partition coefficient for magnesium into aragonite of 0.0013 (Gaetani and Cohen 2006). In the experiments of Morse et al. (1997), a seawater solution with such a Mg/Ca ratio would precipitate aragonite if temperatures were >~14 °C, which is in good agreement with the previous estimates. It may also be relevant to note that Nakamura et al. (2003) described aragonite (although not calcite) in the carbonate-rich lithology of Tagish Lake, an intermediate CI-CM2 carbonaceous chondrite, which they concluded could have formed in contact with magnesium-rich solutions at >50 °C.

This hypothesis for a transition within the Murray parent body from crystallization of calcite to aragonite with an increase in solution Mg/Ca is also consistent with models for the evolution of fluid chemistry within CM2 parent body (or bodies) (Tomeoka and Buseck 1985; Browning et al. 1996; Hanowski and Brearley 2001). By analyzing CMs that have undergone various degrees of aqueous alteration, these studies have shown that matrix cronstedtite recrystallized to Mg-serpentine in response to liberation of magnesium from olivine and pyroxene with progressive parent body aqueous alteration. Thus with time pore fluids became enriched in Mg, although a proportion of it was being simultaneously scavenged by the recrystallizing phyllosilicates. Importantly, Riciputi et al. (1994) showed that solution calcium concentrations did not increase in step with magnesium because the calculated Mg/Ca values of fluids in equilibrium with calcite during its growth (or recrystallization) were greater in the more highly aqueously altered CM2s (mean molar Mg/Ca values of Boreskino = 0.03, Allan Hills (ALH) 83100 = 0.07, Murchison = 0.09 and Nogoya = 0.20) and were greater still during subsequent dolomite precipitation (Boriskino = 2.84; Nogoya = 2.48). The molar Mg/Ca value calculated for solutions in equilibrium with Murray calcite (~0.04) correspond well with the range for other CMs listed above and the molar Mg/Ca value for solutions in equilibrium with M29 aragonite (2.92) is consistent with them becoming more dolomite-like with progressive alteration. As aragonite is clearly rare in the CM2s but occurs in meteorites that have undergone different degrees of aqueous alteration (i.e., Murchison CM2.5, Murray CM2.4/2.5, Cold Bokkeveld CM2.2; Rubin et al. 2007) the conditions suitable for crystallization of aragonite may have been achieved only briefly and the mineral could have been dissolved and/or replaced in those meteorites within which alteration had progressed further. Zolensky et al. (1997) found good evidence within a suite of CM2-CM1 meteorites for such a cycle of carbonate deposition (CM2s) and dissolution (CM1s) with greater degrees of aqueous alteration.

Distribution of Aragonite Forming Solutions

The clustering of aragonite crystals in a small part of each thin section suggests that they grew within films of $CaCO_3$-saturated solutions and the crystals were not subsequently redistributed over a significant scale (i.e., greater than a few tens or hundreds of micrometers) by brecciation or regolith gardening. Thus following crystallization of calcite there must have been a marked reduction in the volume of aqueous fluids present, or at least fluids with a composition suitable for crystallization of aragonite. The most likely explanation for the development of these clusters, which may also be linked to their elongation, is that the distribution of the aragonite-supersaturated fluid films was controlled by a fabric in the matrix and specifically the solutions were focused in narrow zones of a relatively high porosity and permeability. Weak fabrics have been previously identified in a number of carbonaceous chondrites. For example, using X-ray goniometry Fujimura et al. (1983) found that the {001} planes of phyllosilicates in Murchison and Y-74662 (both CM2) have a weak preferred orientation with platy crystals oriented sub-parallel to the plane of uniaxial compression, which attained ~10%. Using EBSD Watt et al. (2006) also described a weak fabric in Allende (CV3) that was expressed by the preferred orientation of platy olivines, but it is important to note that each pole figure they used contained data from 300–700 crystals, far more than were available to the present study. Watt et al. (2006) concluded that the Allende fabric was compaction-related but did not distinguish the relative importance of static (gravitational) and dynamic (impact-related) processes. By contrast Zolensky et al. (1997) suggested from comparisons with terrestrial soils that such fabrics may simply be a by-product of expansion-contraction cycles during aqueous alteration. Evidence for a fabric in Murray includes the elongation of clumps of serpentine-tochilinite in P13115, which are oriented parallel to the long axis of the aragonite cluster. This fabric may have been generated by compaction, for which there is good evidence in the deformation of fine-grained rims and fracturing of M57, both along an axis oriented at a high angle to the serpentine-tochilinite defined fabric. The preferred orientations of aragonite crystals in both clusters could reflect their crystallization within the same static stress field that generated the fabric or may be because there was less resistance to crystal growth parallel rather than normal to the fabric. An alternative possibility is that the aragonite crystals were aligned and the clusters strung out by shearing within the matrix, which is a process that was highlighted by Trigo-Rodríguez et al. (2006) in connection with the origin of fine-grained rims in CM2 meteorites. This explanation is considered less likely than a fabric control on crystal orientations and distributions because if an initially randomly oriented population of aragonite crystals is assumed, some would need to have been rotated by tens of degrees during shearing and it is unlikely that they would have remained as intact as is observed throughout such a process.

CONCLUSIONS

The aragonite crystals in Murray record a period relatively late in the aqueous alteration history of the parent body when a few films of relatively magnesium rich water remained. The marked reduction in the water/rock ratio from the water-saturated matrix within which calcite crystallized and anhydrous silicate, metal and sulfide grains were altered may have been due to consumption of water during hydration reactions coupled with compaction of the matrix and consequent reduction in its porosity and permeability. The fabric of the compacted matrix may also have exerted a strong influence on the orientations of prismatic aragonite crystals growing within the fluid films. Results of this work provide further and unambiguous evidence that water was present within the parent bodies of carbonaceous chondrites and it is likely to have been the primary agent by which most of the hydrous minerals within the matrices, chondrules and CAIs, in addition to the carbonates, were formed. This study has also highlighted the potential for combined petrographic, microstructural and chemical studies of carbonate minerals in carbonaceous chondrites to reveal a wealth of new information on parent body alteration histories.

Acknowledgments–We thank Billy Smith and Colin How for their assistance with the FIB and TEM respectively and Alan Craven for access to facilities in the Department of Physics and Astronomy (Glasgow University). We are also grateful to Paul Edwards (Department of Physics, Strathclyde University) for help with the EPMA and CL spectroscopy and Caroline Smith (NHM, London) for supply of the thin sections and her encouragement. This research was supported by an internship to Rachael Ellen, which was funded by the Paneth Trust of the Royal Astronomical Society. This manuscript was significantly improved by careful reviews from Adrian Brearley, Rachel Beane, and Mike Zolensky.

Editorial Handling—Dr. Adrian Brearley

REFERENCES

Barber D. J. 1981. Matrix phyllosilicates and associated minerals in C2M carbonaceous chondrites. *Geochimica et Cosmochimica Acta* 45:945–970.

Benedix G. K., Leshin L. A., Farquhar J., Jackson T., and Thiemens M. H. 2003. Carbonates in CM2 chondrites: Constraints on alteration conditions from oxygen isotopic compositions and petrographic observations. *Geochimica et Cosmochimica Acta* 67:1577–1588.

Brearley A. J. 1998. Carbonates in CM carbonaceous chondrites: Complex zoning revealed by high resolution

cathodoluminescence studies (abstract #1246). 29th Lunar and Planetary Science Conference. CD-ROM.

Brearley A. J. 2002. Complex zoning in carbonates in CM carbonaceous chondrites: Recorders of changing fluid composition during aqueous alteration? (abstract). 18th Meeting of the International Mineralogical Association.

Brearley A. J. 2006a. The action of water. In *Meteorites and the early solar system II*, edited by Lauretta D. S. and McSween H. Y. Jr. Tucson: The University of Arizona Press. 942 p.

Brearley A. J. 2006b. The role of microchemical environments in the alteration of CM carbonaceous chondrites (abstract #2074). 37th Lunar and Planetary Science Conference. CD-ROM.

Brearley A. J. and Hutcheon I. D. 2002. Carbonates in the Y-791198 CM2 chondrite: zoning and Mn-Cr systematics (abstract). *Meteoritics & Planetary Science* 37:A23.

Brearley A. J., Saxton J. M., Lyon I. C., and Turner G. 1999. Carbonates in the Murchison CM chondrite: CL characteristics and oxygen isotopic compositions (abstract #1301). 30th Lunar and Planetary Science Conference. CD-ROM.

Brearley A. J., Hutcheon I. D., and Browning L. 2001. Compositional zoning and Mn-Cr systematics in carbonates from the Y-791198 CM2 carbonaceous chondrite (abstract #1458). 32nd Lunar and Planetary Science Conference. CD-ROM.

Browning L. B., McSween H. Y., and Zolensky M. E. 1996. Correlated alteration effects in CM carbonaceous chondrites. *Geochimica et Cosmochimica Acta* 60:2621–2633.

Bunch T. E. and Chang S. 1980. Carbonaceous chondrites-II: carbonaceous chondrite phyllosilicates and light element geochemistry as indicators of parent body processes and surface conditions. *Geochimica et Cosmochimica Acta* 44: 1543–1577.

Carlson W. D. 1980. The calcite-aragonite equilibrium—Effects of Sr substitution and anion orientational disorder. *American Mineralogist* 65:1252–1262.

Clayton R. N. and Mayeda T. K. 1999. Oxygen isotope studies of carbonaceous chondrites. *Geochimica et Cosmochimica Acta* 63: 2089–2104.

Conolly S., Smith C. L., Lee M. R., and Benedix G. K. 2007. Carbonate crystallography in the carbonaceous chondrites—A new indicator of impact shock? (abstract). *Meteoritics & Planetary Science* 42:A32.

De Leuw S., Rubin A. E., and Wasson J. T. 2007. Manganese-rich alteration phases in the CM chondrites of different petrographic subtypes: Implications for the timing of aqueous alteration (abstract #1361). 38th Lunar and Planetary Science Conference. CD-ROM.

DuFresne E. R. and Anders E. 1962. Chemical evolution of the carbonaceous chondrites. *Geochimica et Cosmochimica Acta* 26: 1085–1114.

Edwards P. R., Martin R. W., and Lee M. R. 2007. Combined cathodoluminescence hyperspectral imaging and wavelength dispersive X-ray analysis of minerals. *American Mineralogist* 92:235–242.

Fernández-Diaz L., Putnis A., Prieto A., and Putnis C. V. 1996. The role of magnesium in the crystallization of calcite and aragonite in porous medium. *Journal of Sedimentary Research* 66:482–491.

Frisia S., Borsato A., Fairchild I. J., McDermott F,. and Selmo E. M. 2002. Aragonite calcite relationships in speleothems (Grotte de Clamouse, France): Environment, fabrics, and carbonate geochemistry. *Journal of Sedimentary Research* 72:687–699.

Fuchs L. H., Olsen E., and Jensen K. J. 1973. Mineralogy, mineral chemistry and composition of the Murchison (C2) meteorite. *Smithsonian Contributions to Earth Science* 10:1–39.

Fujimura A., Kato M., and Kumazawa M. 1983. Preferred orientation of phyllosilicate [001] in the matrix of Murchison meteorite and possible mechanisms of generating the oriented texture in chondrites. *Earth and Planetary Science Letters* 66:25–32.

Gaetani G. A. and Cohen A. L. 2006. Element partitioning during precipitation of aragonite from seawater: A framework for understanding paleoproxies. *Geochimica et Cosmochimica Acta* 70:4617–4634.

Guo W. and Eiler J. M. 2007. Temperatures of aqueous alteration and evidence for methane generation on the parent bodies of the CM chondrites. *Geochimica et Cosmochimica Acta* 71: 5565–5575.

Grady M. M., Wright I. P., Swart P. K., and Pillinger C. T. 1988. The carbon and oxygen isotopic composition of meteoritic carbonates. *Geochimica et Cosmochimica Acta* 52:2855–2866.

Hanowski N. P. and Brearley A. J. 2000. Iron-rich aureoles in the CM carbonaceous chondrites, Murray, Murchison and ALH 81002: Evidence for in situ aqueous alteration. *Meteoritics & Planetary Science* 35:1291–1308.

Hanowski N. P. and Brearley A. J. 2001. Aqueous alteration of chondrules in the CM carbonaceous chondrite, Allan Hills 81002: Implications for parent body alteration. *Geochimica et Cosmochimica Acta* 65:495–518.

Heaney P. J., Vicenzi E. P., Giannuzzi L. A., and Livi K. J. T. 2001. Focused ion beam milling: A method of site-specific sample extraction for microanalysis of Earth and planetary materials. *American Mineralogist* 86:1094–1099.

Johnson C. A. and Prinz M. 1993. Carbonate compositions in CM and CI chondrites, and implications for aqueous alteration. *Geochimica et Cosmochimica Acta* 57:2843–2852.

Kerridge J. F. and Bunch T. E. 1979. Aqueous activity on asteroids: Evidence from carbonaceous chondrites. In *Asteroids,* edited by Gehrels T. Tucson: The University of Arizona Press. 1181 p.

Lee M. R. and Smith C. L. 2006. Scanning transmission electron microscopy using a SEM: Applications to mineralogy and petrology. *Mineralogical Magazine* 70:561–572.

Lee M. R. and Greenwood R. C. 1994. Alteration of calcium-aluminium-rich inclusions (CAIs) in the Murray (CM2) carbonaceous chondrite. *Meteoritics* 29:780–790.

Lee M. R., Bland P. A., and Graham G. 2003 Preparation of TEM samples by focused ion beam (FIB) techniques: Applications to the study of clays and phyllosilicates in meteorites. *Mineralogical Magazine* 67:581–592.

Lee M. R., Martin R. W., Trager-Cowan C., and Edwards P. R. 2005. Imaging of cathodoluminescence zoning in calcite by scanning electron microscopy and hyperspectral mapping. *Journal of Sedimentary Research* 75:313–322.

Lee M. R., Brown D. J., Smith C. L., Hodson M. E., MacKenzie M., and Hellmann R. 2007. Characterization of mineral surfaces using FIB and TEM: A case study of naturally weathered alkali feldspars. *American Mineralogist* 92:1383–1394.

Marshall D. J. 1988. *Cathodoluminescence of geological materials*. Boston: Unwin Hyman. 146 p.

McSween H. Y. 1979a. Are carbonaceous chondrites primitive or processed? A review. *Reviews in Geophysics and Space Physics* 17:1059–1078.

McSween H. Y. 1979b. Alteration in CM carbonaceous chondrites inferred from modal and chemical variations in matrix. *Geochimica et Cosmochimica Acta* 43:1761–1770.

Metzler K., Bischoff A., and Stöffler D. 1992. Accretionary dust mantles in CM chondrites: Evidence for solar nebula processes. *Geochimica et Cosmochimica Acta* 56:2873–2897.

Morse J. W., Wang Q., and Tsio M. Y. 1997. Influences of

temperature and Mg:Ca ratio on $CaCO_3$ precipitates from seawater. *Geology* 25:85–87.

Müller W. F., Kurat G., and Kracher A. 1979. Chemical and crystallographic study of cronstedite in the matrix of the Cochabamba (CM2) carbonaceous chondrite. *Tschermaks Mineralogische und Petrographische Mitteilungen* 26:293–304.

Nakamura T., Noguchi T., Zolensky M. E., and Tanaka M. 2003. Mineralogy and noble-gas signatures of the carbonate-rich lithology of the Tagish Lake carbonaceous chondrite: Evidence for an accretionary breccia. *Earth and Planetary Science Letters* 207:83–101.

Riciputi L. R., McSween H. Y. Jr., Johnson C. A., and Prinz M. 1994. Minor and trace element concentrations in carbonates of carbonaceous chondrites, and implications for compositions of co-existing fluids. *Geochimica et Cosmochimica Acta* 58:1343– 1351.

Rosenberg N. D., Browning L., and Bourcier W. L. 2001. Modeling aqueous alteration in CM carbonaceous chondrites. *Meteoritics & Planetary Science* 36:239–244.

Rubin A. E. and Wasson J. T. 1986. Chondrules in the Murray CM2 meteorite and compositional differences between CM-CO and ordinary chondrite meteorites. *Geochimica et Cosmochimica Acta* 50:307–315.

Rubin A. E., Trigo-Rodríguez J. M., Huber H., and Wasson J. T. 2007. Progressive aqueous alteration of CM carbonaceous chondrites. *Geochimica et Cosmochimica Acta* 71:2361–2382.

Tomeoka K. and Buseck P. R. 1985. Indicators of aqueous alteration in CM carbonaceous chondrites: Microtextures of a layered mineral containing Fe, S, O, and Ni. *Geochimica et Cosmochimica Acta* 49:2149–2163.

Trigo-Rodríguez J. M. and Wasson J. T. 2006. Non-nebular origin of dark mantles around chondrules and inclusions in CM meteorites. *Geochimica et Cosmochimica Acta* 70:1271–1290.

Watt L. E., Bland P. A., Prior D. J., and Russell S. S. 2006. Fabric analysis of Allende matrix using EBSD. *Meteoritics & Planetary Science* 41:989–1001.

Zolensky M. E. 2001. Asteroidal water: The evidence from the aqueous alteration exhibited by chondritic meteorites (abstract #3052). 11th V. M. Goldschmidt Conference. CD-ROM.

Zolensky M., Barrett R., and Browning L. 1993. Mineralogy and composition of matrix and chondrule rims in carbonaceous chondrites. *Geochimica et Cosmochimica Acta* 57:3123–3148.

Zolensky M. E., Mittlefehldt D. W., Lipschutz M. E., Wang M. S., Clayton R. N., Mayeda T. K., Grady M. M., Pillinger C., and Barber D. 1997. CM chondrites exhibit the complete petrologic range from type 2 to 1. *Geochimica et Cosmochimica Acta* 61: 5099–5115.